Published online 16 October 2022

Nucleic Acids Research, 2022, Vol. 50, No. 22 ***e130***
https://doi.org/10.1093/nar/gkac869

HiFENS: high-throughput FISH detection of endogenous pre-mRNA splicing isoforms

Asaf Shilo[1], Gianluca Pegoraro[2] and Tom Misteli[1,*]

[1]Cell Biology of Genomes, Center for Cancer Research (CCR), National Cancer Institute, NIH, Bethesda, MD 20892, USA and [2]High-Throughput Imaging Facility (HiTIF), Center for Cancer Research (CCR), National Cancer Institute, NIH, Bethesda, MD 20892, USA

Received April 19, 2022; Revised September 01, 2022; Editorial Decision September 23, 2022; Accepted September 27, 2022

ABSTRACT

Splicing factors play an essential role in regulation of alternative pre-mRNA splicing. While much progress has been made in delineating the mechanisms of the splicing machinery, the identity of signal transduction pathways and upstream factors that regulate splicing factor activity is largely unknown. A major challenge in the discovery of upstream regulatory factors of pre-mRNA splicing is the scarcity of functional genomics screening methods to monitor splicing outcomes of endogenous genes. Here, we have developed HiFENS (high throughput FISH detection of endogenous splicing isoforms), a high-throughput imaging assay based on hybridization chain reaction (HCR) and used HiFENS to screen for cellular factors that regulate alternative splicing of endogenous genes. We demonstrate optimized detection with high specificity of endogenous splicing isoforms and multiplexing of probes for accurate detection of splicing outcomes with single cell resolution. As proof-of-principle, we perform an RNAi screen of 702 human kinases and identify potential candidate upstream splicing regulators of the *FGFR2* gene. HiFENS should be a useful tool for the unbiased delineation of cellular pathways involved in alternative splicing regulation.

INTRODUCTION

mRNA transcripts are extensively processed co- and post-transcriptionally, including by polyadenylation at the 3′ end and capping by methyl guanosine at the 5′ end (1–3). One of the major maturation steps for most mRNAs is the excision of non-coding introns during pre-mRNA splicing (4,5). In this process, introns are recognized and marked for removal by cis-acting factors and exons are joined together by the spliceosome to form the mature mRNA.

In addition to the constitutive splicing process, pre-mRNA splicing generates alternatively spliced transcripts by combinatorial use of splice sites (5). Alternative use of 5′ or 3′ splice sites, alternative promoters or polyadenylation sites, or inclusions of introns generates distinct RNA isoforms and leads to diversity at the level of mRNA and ultimately in the proteome (6). One notable form of alternative splicing (AS) is mutually exclusive usage of multiple exons (7,8). In this instance, two or more exons exist in the pre-mRNA but only one of the two is included in the mature mRNA. AS is estimated to occur in more than 90% of human genes and has been suggested to account for at least 10% of disease mutations (9).

Constitutive splicing and AS are tightly regulated, multistep processes (10). Extensive efforts in the past decades have resulted in the detailed characterization of the splicing machinery (10,11). Splicing outcomes are determined by many factors, acting in both *cis* and *trans* (12). Much of the regulatory information is encoded by the mRNA molecule itself, which contains *cis*-acting regulatory elements within its sequence and secondary structure. Short sequences and motifs mark exon-intron boundaries and are directly recognized by trans-acting components of the splicing machinery (5). Additional exonic and intronic regulatory motifs serve as binding sites for splicing factors, which in turn recruit or repel the catalytic splicing machinery of the spliceosome (13). Splicing factor abundance, localization, and activity state are all fundamental for determining splicing outcomes and are responsible for creating different splicing patterns in different cells and tissues.

The activity of splicing factors is affected by post-translational modifications (14). Several kinases that post-translationally modify splicing factors have been identified and include members of the SRPKs (SR protein kinases) and CLKs (cdc2-like kinases) families as well as topoisomerase 1 (TOP1), PRP4 and AKT (15,16). Yet, relatively little is known about other upstream regulatory mechanisms, such as cellular signal transduction pathways, which control the function of splicing factors and thus splicing outcomes (17).

*To whom correspondence should be addressed. Tel: +1 240 670 6669; Fax: +1 240 670 6670; Email: mistelit@mail.nih.gov

A prominent model system for the study of alternative splicing is the human *FGFR2* (fibroblast growth factor receptor 2) gene (18–21). FGFR2 is a tyrosine kinase receptor of the FGFR family and plays a key role in cell division, differentiation, bone and blood vessel development, wound healing, embryonic development, and cancer progression by contributing to epithelial to mesenchymal transition (EMT) (22). *FGFR2* exhibits a prominent splicing pattern depending on cell identity: epithelial cells solely express the *FGFR2*-IIIb isoform, while mesenchymal cells exclusively express the *FGFR2*-IIIc isoform, differing by a mutually exclusive exon in the IgIII loop (23,24) (Figure 1A). The two FGFR2 receptor isoforms differ in ligand binding affinity, which leads to discrete cellular signal transduction events in their physiological context (23). Notably, FGFR2-IIIc is associated with tumor progression and invasiveness, while FGFR2-IIIb has anti-oncogenic activity in bladder and prostate cancers (25,26). Several splicing factors have been identified to play a role in regulation of the FGFR2 AS switch, including ESRP1/2 (Epithelial splicing regulatory protein 1/2) and the histone binding protein MRG15 (MORF-related gene 15) (27–30). In particular, inclusion of *FGFR2*-IIIb is regulated by ESRP1/2 as demonstrated by *in vitro* experiments, use of minigene systems, and analysis of endogenous splicing (31). The identity of additional upstream regulatory factors and of the signaling pathways that orchestrate this switch are largely unknown.

Traditional tools to study AS regulation often include minigenes, which are artificial expression systems that seek to recapitulate the specific AS event of interest. While many insightful discoveries have been made using minigenes (32,33), these systems often only partially recapitulate endogenous splicing patterns (34). Alternatively, investigating AS regulation using endogenous RNAs can be done using sequencing methods. However, these approaches are generally not suitable for high throughput assays needed to perform screens to identify novel regulatory factors in a systematic and unbiased fashion. For this reason, high-throughput quantitative assays are needed to measure endogenous splicing outcomes in functional genomics screens.

High-throughput imaging (HTI) assays can be used to simultaneously perturb a large number of genes in parallel, using small molecules, RNAi, or CRISPR/Cas9, offering a potential mean to identify novel splicing regulators (35). However, HTI-based minigene reporters to quantitatively detect AS changes may not fully reflect *in vivo* behavior of the full length endogenous pre-mRNA (36). Several HTI-based methods such as single molecule RNA FISH (smFISH) have emerged recently (37), yet smFISH is generally not sensitive enough to detect small mRNA targets (50 – 500 nt), such as small exons or specific splice junctions, which is needed to measure changes in AS patterns. In addition, smFISH usually requires high magnification and high NA objectives, which limit the size of each field of view imaged, and, as a consequence, reduce the throughput of the assay.

The recent development of ultrasensitive *in-situ* detection methods offers new opportunities for the single-cell analysis of splicing isoforms (38). In particular, Hybridization Chain Reaction (HCR) (39,40) has allowed detection of low expression genes or short RNA sequences using a signal amplification step via two sets of DNA hairpins (41). HCR offers increased sensitivity and quantitative detection of RNA molecules *in situ*, and it can be adapted to lower magnification objectives making it compatible with HTI screening (41). Here, we have exploited HCR-mediated detection of short RNA sequences to assess alternative splicing in *FGFR2*. By integrating HCR into a HTI pipeline we have developed HiFENS (high-throughput FFISH detection of endogenous splicing isoforms), a method for the quantitative detection of endogenous RNA splicing variants in a high-throughput format and for the discovery of upstream regulators of alternative splicing. We optimize and validate the method, and, using *FGFR2* as a model system, demonstrate proof-of-principle of its use in RNAi screening.

MATERIALS AND METHODS

Cell culture and transfection conditions

MCF7 cells were cultured in EMEM (ATCC) supplemented with 10% FBS (Sigma) and 0.01 mg/ml human recombinant insulin (Life Technologies). T-47D and SN12C (NCI Division of Cancer Treatment and Diagnosis Tumor Repository) cells were cultured in RPMI-1640 Medium (Life Technologies) supplemented with 10% FBS (Sigma). AN3-CA cells were cultured in MEM (Life Technologies) supplemented with 10% FBS (Sigma). Normal human fibroblast cells (CRL-1474) were cultured in MEM (Life Technologies) supplemented with 15% FBS (Sigma). MCF-10A and MCF-10AT1k.cl2 (MCF10AT) cells were provided by Dan Levy (University of Wyoming) and cultured in DMEM/F12 (1:1) (Life Technologies), 1.05 mM $CaCl_2$, 4.9% horse serum, 10 mM HEPES, 10 μg/ml insulin, 20 ng/ml EGF, and 0.5 μg/ml hydrocortisone and 0.1 μg/ml cholera toxin. HEK293T and U2OS cells were cultured in DMEM (Life Technologies) supplemented with 10% FBS (Sigma). All cells were supplemented with 2 mM l-glutamine, 1 mM sodium pyruvate, non-essential amino acids, 100 U/ml penicillin and 100 μg/ml streptomycin (Life Technologies) and cultured at 37°C and 5% CO_2. Unless indicated otherwise, cell lines were purchased from ATCC.

Plasmids and virus production

Mammalian expression vectors for *FGFR2*-IIIb (pBp-FGFR2b-WT, Addgene plasmid # 45698), *FGFR2*-IIIc (pBp-FGFR2c-WT, Addgene plasmid # 45699) and empty vector (pBABE-puro, Addgene plasmid # 51070) were used. To generate stable cell lines, HEK293T cells were transfected using linear-polyethylenimine (Sigma) with pBABE-puro retroviral vectors expressing the indicated cDNAs together with pGAGpol and VSV-G. Virus containing media was collected 48 h after transfection and filtered. Polybrene (Sigma) was added to filtered virus media before it was added to U2OS cells. Twenty-four hours later, U2OS media was replaced with fresh media and 24 h later U2OS infected cells were selected with 2 μg/ml of puromycin (InvivoGen) for 72 h.

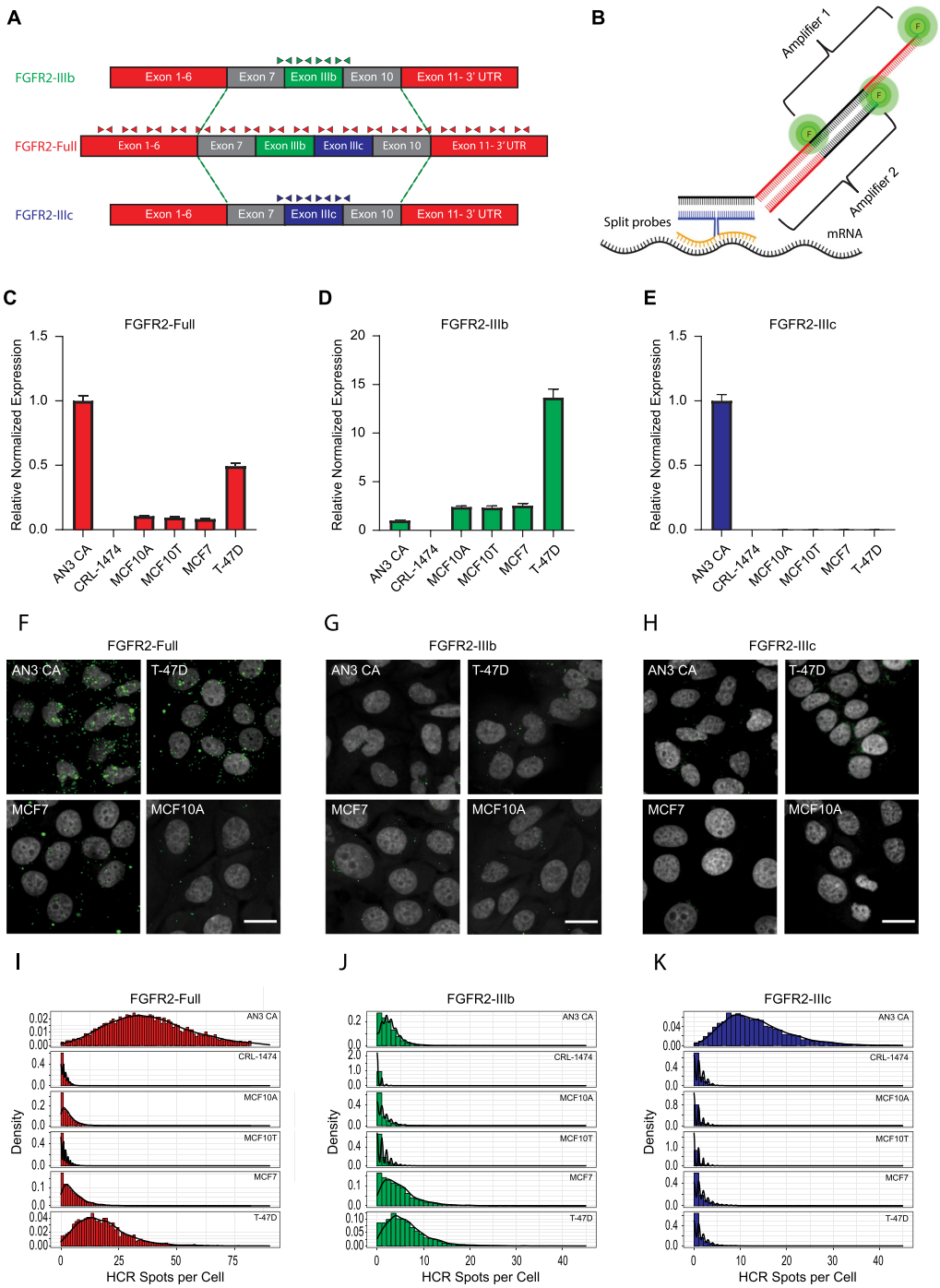

Figure 1. Quantitative Measurement of *FGFR2* Isoforms by qRT-PCR and RNA-HCR-FISH. (**A**) Schematic representation of the mutually exclusive *FGFR2* splicing event and HCR probe pair location. Boxes indicate exons. Numbers and letters indicate exons number or name. Red boxes represent exons located upstream and downstream of the splicing cassette. Grey boxes represent the constitutive flanking exons 7 and 10. Green and blue boxes represent exon IIIb or exon IIIc, respectively, whose inclusion led to formation of the *FGFR2*-IIIb or *FGFR2*-IIIc isoforms, respectively. Triangles over the boxes represents RNA-HCR-FISH probe locations. Green represents *FGFR2*-IIIb specific probes, red represents *FGFR2*-Full probes, blue represents *FGFR2*-IIIc specific probe locations. (**B**) RNA-HCR-FISH. The black curved line represents the mRNA target molecule, Orange curved lines represent split probes. The blue line represents the linker, while the blue dashed curved line represents the initiator. Black and red lines represent the fluorescently labeled amplifiers in an open state. (**C–E**) Quantitative RT-PCR for *FGFR2*-Full (C), *FGFR2*-IIIb (D) and *FGFR2*-IIIc (E) isoforms from the indicated cell lines. Expression levels are normalized to expression of TBP, and relative to the expression in AN3 CA cells which was arbitrarily set at one. Note the differences in the scale of the Y axes. Values represent mean ± SEM of three replicates. (**F–H**) Representative fields of view of RNA-HCR-FISH for *FGFR2*-Full (F), *FGFR2*-IIIb (G) and *FGFR2*-IIIc (H). Indicated cell lines were seed on 384-well plates and 24 h later were subjected to RNA-HCR-FISH (Scale bar: 20 μm). (**I–K**) Histogram and density plot of RNA-HCR-FISH quantitative spot count measurements for *FGFR2*-Full (I), *FGFR2*-IIIb (J) and *FGFR2*-IIIc (K) isoforms in the indicated cell lines. Values are generated from single cell data and are representative of four replicates. At least 700 cells were analyzed per sample.

siRNA transfection

3.5×10^5 T-47D cells were plated on a 6-well plate 24 h before transfection. Transfections were performed using DharmaFECT1 transfection reagent (Horizon Discoveries), as per manufacturer instructions. Cell were incubated for 72 h with a final siRNA oligo concentration of 25 nM. The siRNA oligos used were Silencer Select negative control (Ambion, #4390846), Silencer Select ESRP1 siRNA (Ambion, # 4392420, ID: s29570), Silencer Select ESRP2 siRNA (Ambion, # 4392420, ID: s228220). For screen validation, a custom siRNA library was purchased from Horizon Discoveries. For each gene, four individuals OnTarget Plus siRNAs were pooled.

RNA isolation and qRT-PCR analysis

RNA was isolated from cell culture samples at 72 h post transfection using NucleoSpin RNA Plus (Machery Nagel). 1 μg of each RNA sample was reverse transcribed to cDNA using the iScript cDNA synthesis kit (Bio-Rad). Quantitative PCR was performed on cDNA samples using the iQ SYBRGreen Supermix (Bio-Rad) on a CFX96 Real Time PCR System (Bio-Rad) to measure *FGFR2*-Full, *FGFR2*-IIIb, *FGFR2*-IIIc and TATA-binding protein (*TBP*). The qPCR protocol consisted of 3 min at 95°C, 40 cycles of 20 s at 95°C, and 30 s at 58°C. Reactions were performed in triplicate. Analysis was performed using the Bio-Rad CFX Maestro Software. *FGFR2*-Full, *FGFR2*-IIIb, *FGFR2*-IIIc expression levels were normalized to expression of *TBP*. Data are displayed as mean expression values ± SEM. Primers sequence are provided in Supplementary Table S1.

RNA-HCR probes and amplifiers

All HCR probes, amplifiers and buffers were purchased form Molecular Instruments. Lot numbers for probes used in this study: FGFR2-Full-2584/B531, FGFR2-NTC-PRA272, FGFR2-3′-PRH048, FGFR2 5′-PRH047, FGFR2-IIIb-PRA269, FGFR2-IIIc-PRA270, TBP-PRB521, PGK1-3059/C021, ESRP1- PRD708, ESRP2-PRD709. Probes for *FGFR2*-IIIb, *FGFR2*-IIIc, *FGFR2*-D7-10, *FGFR2*-5′ and *FGFR2*-3′ were all custom designed for this study. Unless specified, B1 probes were used with amplifier B1-Alexa Flour 488 and B3 probes with B3-Alexa Fluor 647 (Molecular Instruments). B2 probes were custom designed for amplification with B2- Alexa Fluor 562 (Molecular Instruments). The amplification protocol was performed according to manufacturer instructions. *FGFR2*-IIIb/c probes were used at 10 nM final concentration. *FGFR2*-Full and *TBP* probes at 2 nM. Amplifiers were used at 60 nM for isoform detection and at 30 nM for all other targets.

High throughput siRNA transfection in 384-well format

The Invitrogen™ Silencer™ Human Kinase siRNA Library containing 2127 total siRNAs targeting 702 genes was used. siRNAs were resuspended as 5 μM stock in ddH2O, diluted to 400 nM, and 150 nl of each diluted siRNA were spotted at the bottom of 384-well CellCarrier Ultra imaging plates (PerkinElmer, #6057300) using the ECHO525 acoustic liquid dispenser (Labcyte). For the entire library six 384-well plates were spotted. 150 nl of 400 nM siRNA oligos of a negative, nontargeting control siRNA (*Silencer*™ Select Negative Control No. 2 siRNA; Invitrogen), a positive control siRNA (Allstars Hs Cell Death Control siRNA, QIAGEN, #1027298), and two positive biological controls of siRNAs (ESRP1, ESRP2) were spotted in eight replicates for each plate. The 384-well plates were air dried under a sterile laminar flow for at least 30 min, sealed, and then stored at − 30°C until transfection. Reverse siRNA transfections were carried out using DharmaFECT1 transfection reagent (Horizon Discoveries) per the manufacturers' instructions. Transfection reagent and cells were added robotically using a Multidrop Combi dispenser (Thermo Scientific). Transfected cells were incubated for 72 h at 37°C, 5% CO_2.

High-throughput RNA-HCR-FISH in 384-well plates

Cells were treated per the instructions provided by Molecular Instruments (https://files.molecularinstruments.com/MI-Protocol-RNAFISH-MammalianCellSlide-Rev7.pdf) with some modifications. Briefly, cells were fixed in 4% PFA in PBS for 15 min, washed three times with PBS, and permeabilized in 70% ethanol overnight at –20°C using a Blue-Washer dispenser (Blue cat-bio). 10 μl of a probe mix in hybridization buffer (Molecular Instrument) was added using the Mosquito dispenser (Sptlabtech) and left to hybridize at 37°C overnight. Plates were washed four times with wash buffer (Molecular Instrument) at 37°C for 15 min using a Blue-Washer dispenser (Blue cat-bio). 10 μl of amplifiers mix in amplification buffer (Molecular Instrument) was added using a Mosquito dispenser (Sptlabtech) and left at RT for 45 min. Excess Amplifiers were washed with a Blue-Washer five times with 5× SSC with 0.1% Tween-20 for 15 min. Cells were stained with DAPI in PBS (5 ng/μl) before imaging.

High-throughput image acquisition and analysis

Fixed and stained cells were imaged in four channels (405, 488, 561 and 640 nm excitation lasers) in an automated fashion using a dual spinning disk high-throughput confocal microscope (Yokogawa CV7000) with a 40x air objective lens (NA 0.95) and two 16-bit sCMOS cameras with binning set to 2 (Pixel size: 325 nm). We acquired 3D z-stacks of 3-5 μm in each channel, at every 1 μm interval, and maximally projected the images on the fly. 8–12 randomly selected fields of view were imaged per well. Images were corrected on the fly using a Yokogawa proprietary software for correction of camera alignment, optical aberrations, vignetting, and camera background. Maximally projected and corrected images were saved and stored as 16-bit TIFF files.

Cell segmentation and counting

Images were analyzed using Columbus 2.8.1 (PerkinElmer). Automated nucleus segmentation was based on the maximal projection of the DAPI signal (ex. 405 nm) using the

following criteria: common threshold: 0.3, area: >50 μm^2, splitting coefficient: 7, individual threshold: 0.4, contrast: >0.4. Automated cytoplasm detection was based on the maximal projection of the weak cytoplasmic DAPI signal. HCR-RNA-FISH spots within these cells were identified in maximal projections using the green (ex. 488 nm), red (ex. 561 nm) or far- red (ex. 640 nm) channels, using local and global contrast with the following criteria: radius: <3 pixel, contrast: >0.1, uncorrected spot to region intensity: >0.1, region intensity: >2, distance: >2 pixel, spot peak radius: 1 pixel. The radius and distance parameters increase accuracy of detection in case of clusters of spots. Columbus used a linear classifier algorithm that was trained to separate between positive and negative (background) spots for each channel. Only data for positive spots was used for analysis.

Image and data presentation

The original TIFF files were processed in FIJI/ImageJ (NIH) by adjusting brightness and contrast settings over the entire FOV, maintaining them constant across all images in the same figure panel. For merged images, grayscale 16-bit images from different channels were merged and converted to 8-bit RGB format. All imaging and high-throughput data calculations were performed using custom scripts in R software. The R analysis scripts used to generate the plots in the figures are deposited at https://github.com/CBIIT/mistelilab-hifens. Diagrams were created with BioRender (BioRender.com) or with Adobe Illustrator (Adobe). Plots, images and diagrams were combined into figures using Adobe Illustrator (Adobe).

Statistical analysis

Single cell results generated in Columbus were exported into R software (4.1, R Core Team) and RStudio Desktop (RStudio) and analyzed using custom scripts. Statistical tests and *p*-values were calculated using the Kruskal-Wallis test, which extends the Mann-Whitney test to multiple samples followed by a post-hoc Dunn test, to compare the different cell lines between each other or by a Spearman correlation coefficient test for scatter plots. Typically, no fewer than 500 cells were analyzed per sample. qRT-PCR analysis was performed using the Bio-Rad CFX Maestro Software and Prism8 (GraphPad).

RESULTS

FGFR2 splice variant isoform detection by HCR-RNA-FISH

We sought to design HCR-RNA-FISH probes to detect the two mutually exclusive (ME) *FGFR2* isoforms, *FGFR2*-IIIb and *FGFR2*-IIIc, quantitatively and with high sensitivity and specificity in intact cells. Pairs of HCR oligo DNA probes (39) were designed to hybridize to the interior of each *FGFR2* exon and at splice junctions (Figure 1A; see Materials and Methods). Each probe consists of 50 nt complementary to the *FGFR2* target sequence and a split synthetic initiator sequence (Figure 1B). Only when both split probes bind to adjacent regions of the target mRNA is the full initiator sequence formed (Figure 1B). The assembly of the initiator sequence then triggers the unfolding and sequential local oligomerization of fluorescently labelled oligo DNA amplifiers, which when unbound are present in metastable hairpins that can be washed away (39). Limited by the short length of the ME exons (148 nt for *FGFR2*-IIIb, and 145 nt for *FGFR2*-IIIc) and the length of the probes (50 nt per probe), we were only able to design 4 probe pairs for each ME exon variant (Figure 1A). In addition, to detect total *FGFR2* RNA, a set of 18 probe pairs spanning the entire length of the *FGFR2* RNA was generated (Figure 1A).

We first validated the specificity of these probes by comparing measurements of *FGFR2* expression and isoform ratios obtained with qRT-PCR or HCR imaging in multiple cell lines. When analyzed by qRT-PCR, three breast cancer cell lines (MCF7, MCF10A, MCF10AT) exhibited low to moderate expression of full length *FGFR2* mRNA, whereas the breast cancer cell line T-47D showed high expression (Figure 1C). hTERT-immortalized CRL-1474 human fibroblasts did not express *FGFR2* at all, and the adenocarcinoma cell line AN3-CA expressed the highest levels of *FGFR2* of all cell lines tested (Figure 1C). All four breast cancer cell lines (MCF7, MCF10A, MCF10AT and T-47D) are epithelial and, as expected, express only the *FGFR2*-IIIb isoform with T-47D cells containing the highest levels, in line with high levels of total *FGFR2* in these cells (Figure 1D). The *FGFR2*-IIIb isoform was not detectable in CRL-1474 cells (Figure 1C), while *FGFR2*-IIIc was detectable only in AN3-CA (Figure 1E). AN3-CA cells also express some *FGFR2*-IIIb (Figure 1D).

To quantify in parallel RNA abundance by HCR-RNA-FISH, we typically imaged at least 500 cells per well in a 384-well plate format using a fully automated high-throughput microscope (see Materials and Methods). RNA levels were measured by spot counting in individual cells. Spot counting was used because it was more robust than spot intensity measurements, and both methods showed indistinguishable patterns for all measured genes (Figure 1F-H; Supplementary Figure S1; see Materials and Methods). Reassuringly, the HCR-RNA-FISH imaging data matched well the qRT-PCR measurements. Total *FGFR2* spot count was highest in AN3-CA cells (Figure 1F, I) and the spot count in T-47D cells was lower than in AN3-CA, but higher than in MCF7, MCF10A, MCF10AT, and CRL-1474 as observed by qRT-PCR (Figure 1F, I). Similarly, *FGFR2*-IIIb displayed the highest spot count in T-47D cells (Figure 1G, J) and *FGFR2*-IIIc was detected only in AN3-CA cells (Figure 1H, K). These results indicate that qRT-PCR and imaging-based HCR-RNA-FISH measurements for *FGFR2* full length and for its AS isoforms accurately reflect the abundance of isoforms in multiple cell lines across a wide range of expression levels of these mRNA species.

Spot count detection optimization

The probe set for each *FGFR2* isoform consists of four individual probes (Figure 2A; see Materials and Methods). One probe pair is designed to bind to the junction of exon 7 and the ME specific exon (PB1 for *FGFR2*-IIIb, PC1 for *FGFR2*-IIIc) (Figure 2A) and another binds the ME specific exon (PB2 and PB3 for *FGFR2*-IIIb, PC2 and PC3 for

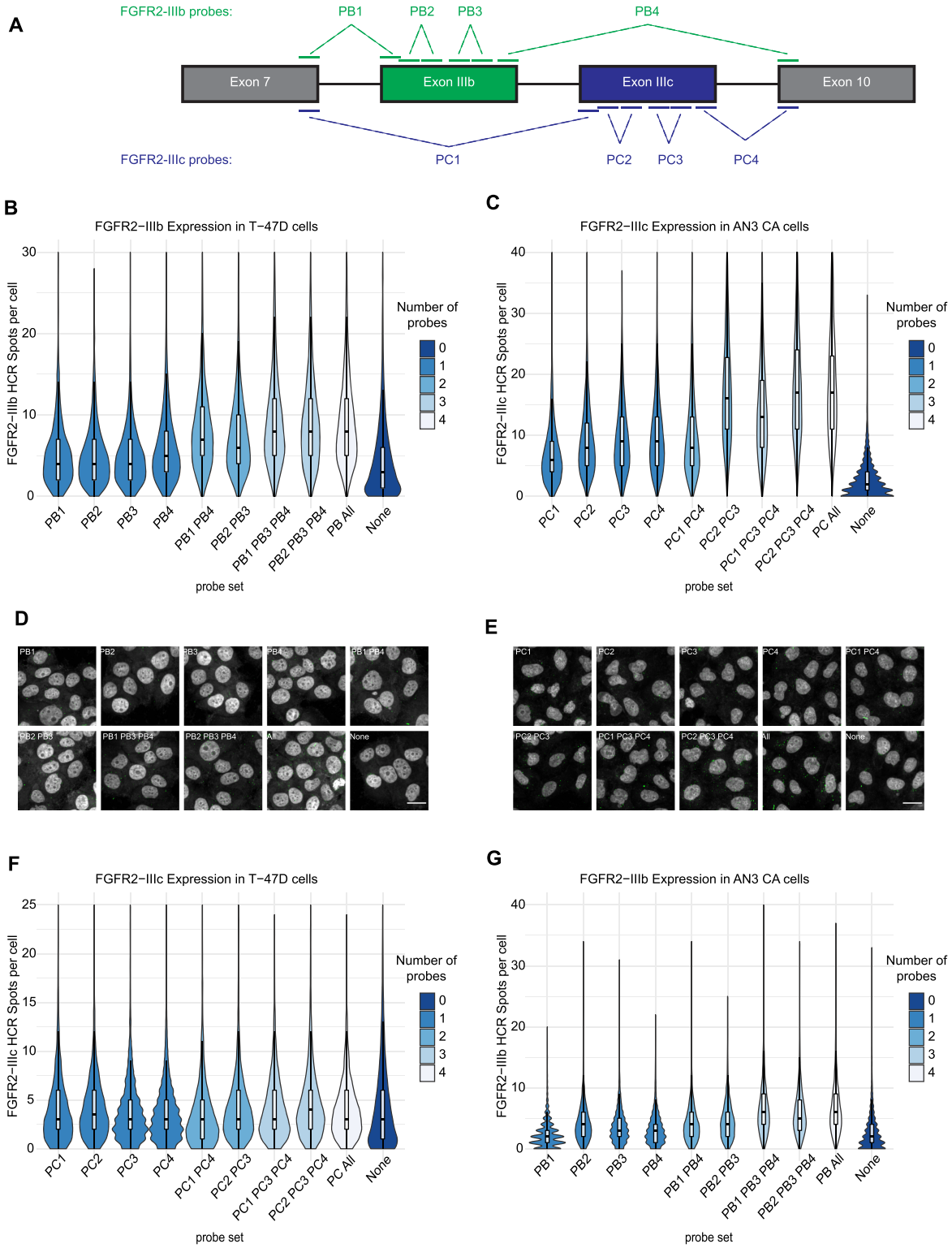

Figure 2. Effect of probe numbers on spot count. (**A**) Schematic representation of *FGFR2* isoform-specific probe locations. Boxes indicate exons. Black lines between boxes indicated introns. Numbers and letters insides boxes indicate exon number or name. Green and blue lines represent exon IIIb or exon IIIc probe locations, respectively. Dashed lines indicate split HCR probes pairs. (**B**, **C**, **F**, **G**) Violin and box plots for spot count measurements for *FGFR2*-IIIb in T-47D cells (B), *FGFR2*-IIIc in AN3-CA cells (C), *FGFR2*-IIIc in T-47D cells (F), or *FGFR2*-IIIb in AN3-CA cells (G) in different combination of probe sets (x-axis). Box plot inside each violin plot indicate the 25th, 50th (median) and 75th percentile of the distributions and whiskers extend to 1.5X the inter-quantile range (IQR). Numbers in legend indicate number of probes per setting. Values are generated from single cell data and are representative of 4 replicates. At least 1000 cells were analyzed per sample. (**D**, **E**) Representative fields of view of RNA-HCR-FISH for *FGFR2*-IIIb in T-47D cells (F) and *FGFR2*-IIIc in AN3-CA cells (G) (scale bar: 20 μm).

FGFR2-IIIc). Each probe set also contains an additional probe pair designed to bind to the junction of the ME specific exon and exon 10 (PB4 for *FGFR2*-IIIb, PC4 for *FGFR2*-IIIc) (Figure 2A). To achieve optimal spot count detection, we compared different combinations of sets of probes. As a control, cells were exposed to buffer only without any probes ('None'). *FGFR2*-IIIb probes were tested in T-47D cells and *FGFR2*-IIIc probe were tested in AN3-CA cells, each of which robustly express either of the two isoforms (Figure 1D, E). Increasing the number of probe pairs in the probe set resulted in higher HCR spot counts in both cases (Figure 2B, C). For T-47D cells, all combinations of three probes were as effective as all four probes combined (Figure 2B). The triplet probe mixtures either lacked the first exonic probe (PB1) or the first junction (PB2) probe (Figure 2B). For AN3-CA cells, only the mixture of three probes without the first junction (PC1) probe was as effective as all 4 probes in combination (Figure 2C). As a control for non-specific detection, *FGFR2*-IIIc probes were tested in *FGFR2*-IIIb expressing T-47D cells and no significant spot count above background was observed (Figure 2D). In line with robust specificity and sensitivity, *FGFR2*-IIIb probes detected this isoform in AN3-CA cells which express only low levels of *FGFR2*-IIIb (Figure 2E). In this case, spot count was also correlated with the number of probes used (Figure 2E). In both T-47D and AN3-CA cells total spot area was correlated with the number of spots, however, spot size was not affected by probe number (Supplementary Figure S2).

HCR-RNA-FISH uses fluorescently labelled hairpin DNA oligos to amplify the FISH signal (39). To optimize the sensitivity of detection, we tested DNA oligo hairpins labelled either with Alexa Flour 488 (green channel) or with Alexa Flour 647 (far red channel), respectively, to detect the same isoform probe sets. Using *FGFR2*-IIIb or *FGFR2*-IIIc specific probes in T-47D cells (Supplementary Figure S3A) or AN3-CA cells (Supplementary Figure S3B), respectively, we found that HCR with Alexa Flour 647-labelled hairpins consistently yielded higher spot counts in our experimental conditions. This discrepancy may be due to higher autofluorescence background signal in the green channel.

Isoform specific HCR-RNA-FISH probes specificity

Next, we determined the specificity of the HCR *FGFR2* isoform probe sets. Plasmids expressing *FGFR2*-IIIb or *FGFR2*-IIIc mRNA were transfected in U2OS cells, and an empty plasmid vector (EV) was used as a negative control. qRT-PCR for total *FGFR2* mRNA and spliced variant isoforms confirmed low endogenous expression of *FGFR2*-IIIc in U2OS cells and exogenous expression with *FGFR2*-IIIb overexpression being more pronounced than *FGFR2*-IIIc (Supplementary Figure S4). As a control for *FGFR2*-IIIb specific probes, we used MCF7 cells which endogenously express only *FGFR2*-IIIb. mRNA expression levels measured by qRT-PCR (Supplementary Figure S4) corresponded well with mRNA spot counts by HCR-RNA-FISH (Figure 3A–C). Total *FGFR2* expression was higher in MCF7 cells than in U2OS EV cells (Figure 3A, D). U2OS cells overexpressing *FGFR2*-IIIb showed higher spot count for both *FGFR2*-full and *FGFR2*-IIIb compared to MCF7, or U2OS expressing *FGFR2*-IIIc or the control EV (Figure 3A, B and D). As expected, *FGFR2*-IIIb specific probes showed no signal in U2OS cells with *FGFR2*-IIIc overexpression or in EV controls (Figure 3B, D). As a control, *PGK1*, a house-keeping gene, had the same expression levels across U2OS cells transfected with the various expression plasmids, demonstrating that changes in *FGFR2* HCR spot counts are due to *FGFR2* overexpression rather than to global changes in gene expression triggered by transfection (Figure 3C, D). Probe specificity was also tested by overexpressing *FGFR2*-IIIb or -IIIc in human kidney renal cell carcinoma SN12C cells, which do not express any endogenous FGFR2 (CellMinerCDB database (https://discover.nci.nih.gov/rsconnect/cellminercdb). qRT-PCR for total *FGFR2* mRNA and spliced variant isoforms confirmed exogenous expression of *FGFR2*-IIIb or *FGFR2*-IIIc with *FGFR2*-IIIb overexpression being more pronounced than *FGFR2*-IIIc (Supplementary Figure S5). Once again, HCR spot count data show similar patterns to expression levels measured by qRT-PCR (Supplementary Figure S6). Altogether, these results show that HCR-RNA-FISH probes for isoform-specific detection of *FGFR2* mRNA are highly specific.

Multiplexing probes for *FGFR2* detection

The calculation of expression ratios for the two isoforms of *FGFR2* as a proxy measurement for AS isoform ratios requires the simultaneous detection of the isoform of interest and the full-length RNA in the same cell using different spectral channels. We were able to use the probe sets for detection of each isoform and total *FGFR2* RNA in a pooled fashion, since each of the three different probes sets carry a different initiator sequence, each of which specifically triggers the polymerization of a cognate pair of hairpins, which are themselves labelled with fluorophores that can be simultaneously imaged in different spectral channels. To optimize multi-channel detection, and to include a house-keeping gene as an internal control, we multiplexed HCR probe sets and their cognate hairpins for detection of total-*FGFR2*, *FGFR2*-IIIb or *PGK1*. A total-*FGFR2*/*FGFR2*-IIIb combination probe rather than a *FGFR2*-IIIb/*FGFR2*-IIIc probe was used because it gives information as to whether changes in isoform detection are due to changes in *FGFR2* RNA expression or stability, which is not possible using the isoforms ratio. In addition, we wanted to exclude any probe interference between *FGFR2*-IIIb and *FGFR2*-IIIc probes which may reduce spot number detection. Since the previously used total-*FGFR2* probes also hybridize to the ME spliced exons, we used a new probe set, *FGFR2*-D7-10, that binds upstream and downstream of the splicing event, thus precluding any potential interference with isoform-specific *FGFR2* probe sets. *FGFR2*-D7-10 probes behaved indistinguishably from total-*FGFR2* probes in multiple cell lines (Supplementary Figure S7). In multiplexing experiments, the HCR spot counts for *FGFR2* (Figure 4A), *FGFR2*-IIIb (Figure 4B), and *PGK1* (Figure 4C) were similar to when the probe sets were used in separate wells. Accurate detection in a multiplexed format was confirmed by strong correlation ($r = 0.87$) between *FGFR2*-IIIb and *FGFR2*-D7-10 HCR spot counts in individual U2OS cells

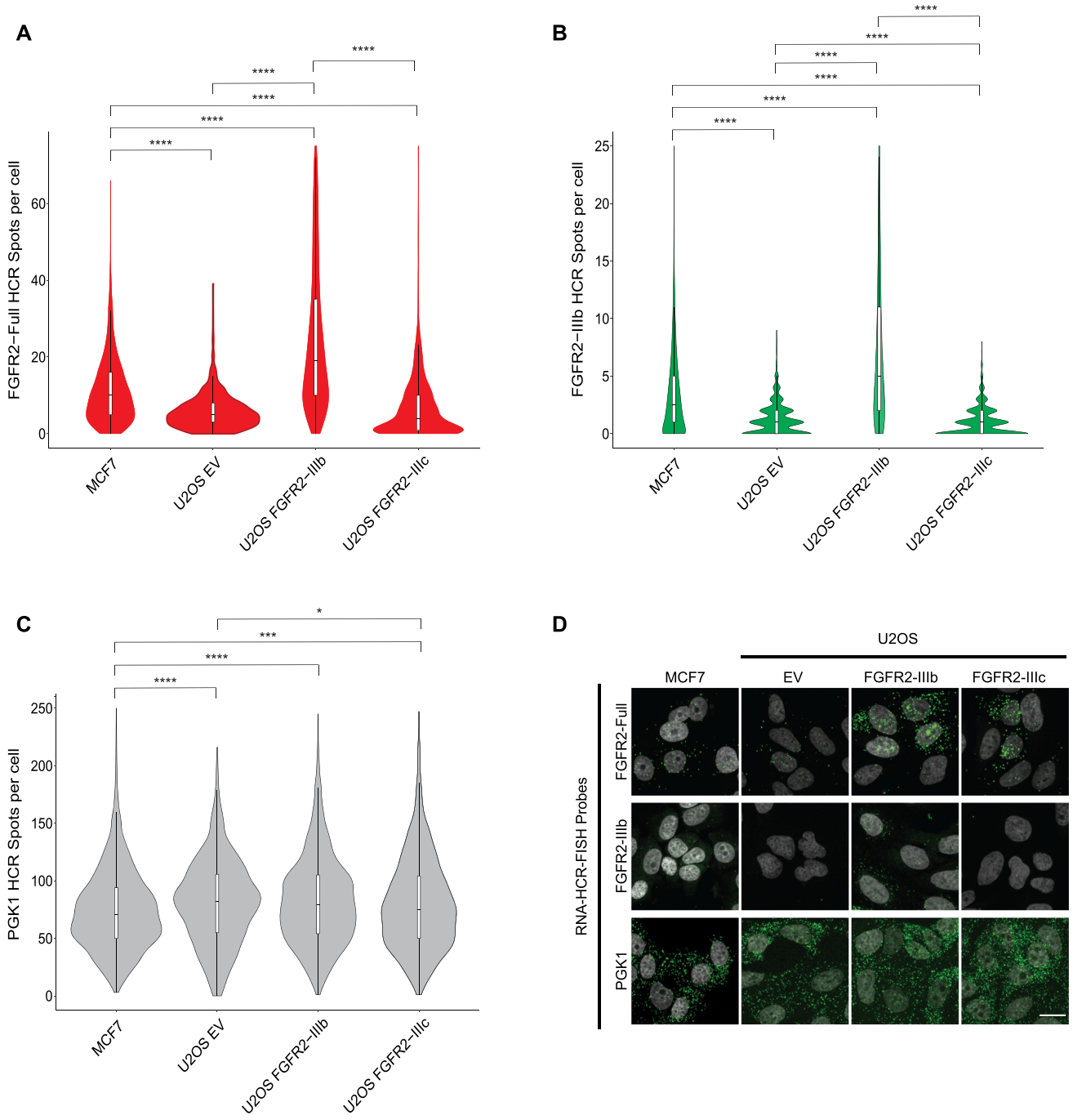

Figure 3. Specific detection of FGFR2 isoforms. (**A–C**) Violin and box plots for single cell RNA-HCR-FISH spot count measurements for *FGFR2*-Full (A), *FGFR2*-IIIb (B) and *PGK1* (C) of each indicated cell line. U2OS cells were infected with virus to overexpress *FGFR2*-IIIb, *FGFR2*-IIIc or empty vector (EV). MCF7 and the above-mentioned cells were fixed and stained with RNA-HCR-FISH. Boxes inside violin plot indicate the 25th, 50th (median) and 75th percentile of the distributions and whiskers extend to 1.5X inter-quantile range (IQR). *$P < 0.05$, ***$P < 0.001$, ****$P < 0.0001$. *P*-values are from a Kruskal–Wallis test, which extends the Mann–Whitney test to multiple samples followed by a post-hoc Dunn test, to compare the different cell lines between each other. Values are generated from single cell data and are representative of three replicates. At least, 500 cells were analyzed per sample. (**D**) Representative field of view of RNA-HCR-FISH spots for FGFR2-Full, FGFR2-IIIb and PGK1 in cell lines described in A–C. Scale bar: 20 μm.

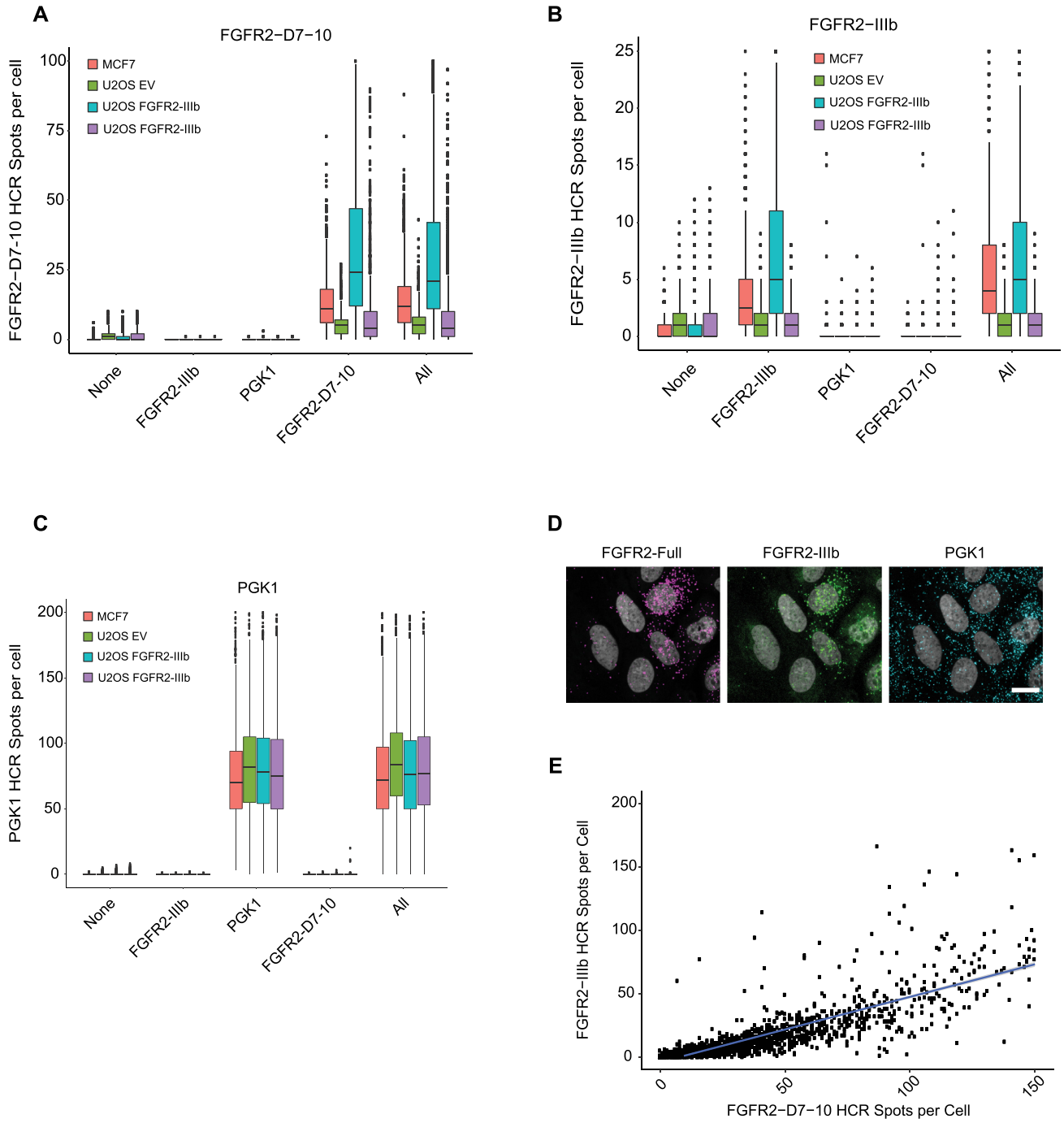

Figure 4. Multiplexing of RNA-HCR-FISH probes. (**A–C**) Box plot for RNA-HCR-FISH spot count measurements for multiplexed probes for *FGFR2*-D7-10 (A), *FGFR2*-IIIb (B) and *PGK1* (C) in cells described in Figure 3. X-axes indicate probe combinations. Boxes show the 25th, 50th (median) and 75th percentile of the distributions and whiskers extend to 1.5X inter-quantile range (IQR), outliers are represented as dots. Values are generated from single cell data and are representative of three replicates. At least 500 cells were analyzed per sample (none: no probes. All: multiplexed probes for *FGFR2*-D7-10, *FGFR2*-IIIb and *PGK1*). (**D**) Representative field of view of RNA-HCR-FISH for *FGFR2*-Full, *FGFR2*-IIIb and *PGK1* in U2OS cell overexpressing *FGFR2*-IIIb. Scale bar: 20 μm. (**E**) Scatter plot of RNA-HCR-FISH spot count measurements for *FGFR2*-D7-10 (x-axis) and *FGFR2*-IIIb (y-axis) in U2OS cells over expressing *FGFR2*-IIIb. Correlation coefficient ($r = 0.87$) and *P*-value ($P < 2.2e{-}16$) are from a Spearman correlation coefficient test.

overexpressing *FGFR2*-IIIb (Figure 4D, E). These results demonstrate that multiplexed HCR measurements serve as a robust indicator of total-*FGFR2* and *FGFR2*-IIIb expression in single cells.

To further confirm the multiplexing ability of the detection approach, we split *FGFR2*-D7-10 probes into two parts and measured total *FGFR2* levels with two probe sets (Supplementary Figure S8). One set was designed to hybridize to exon 1 to 6 of *FGFR2* (*FGFR2* 5′), and its probes contained a split B2 initiator sequence. *FGFR2* 5′ was detected using HCR B2 hairpin oligos with Alexa Fluor 568 that were imaged in the red channel (Supplementary Figure S8A). Another probe set was designed to hybridize to exons 11–18 (*FGFR2* 3′). The probes for this set contained the split B3 initiator sequence that triggers the oligomerization of HCR B3 hairpin oligos labelled with Alexa Fluor 647, which can then be imaged in the far-red channel (Supplementary Figure S8A). HCR spot counts for *FGFR2* 5′ and *FGFR2* 3′ were similar regardless of whether the target gene was probed with only one set or with both probe sets in a multiplexed format (Supplementary Figure S8B, C). Single cell data from the multiplexed probes sets show high correlation between *FGFR2* 5′ spot count and *FGFR2* 3′ spot count ($r = 0.72$), suggesting that both probe sets indeed detect the same molecule (Supplementary Figure S8D). In addition, no signal was observed in the red channel for the *FGFR2* 3′ detected with the Alexa Fluor 568 or in the far-red channel for *FGFR2* 5′ with the Alexa Fluor 647 indicative of high specificity for RNA-HCR-FISH (Supplementary Figure S8E).

Taken together, these results demonstrate accurate detection of specific RNA isoforms with high sensitivity in a multiplexed format using HCR-RNA-FISH on a 384-well high-throughput platform. We refer to this detection pipeline as HiFENS.

Biological controls for FGFR2 splicing

To validate the specificity of isoform detection by HiFENS in a biologically relevant context, we sought to monitor changes of endogenous RNA spliced variant isoforms in response to known biological effectors of *FGFR2* splicing. Splicing of *FGFR2* is known to be regulated, in part, by the ESRP proteins and knock down of *ESRP1* and *ESRP2* in epithelial cells decreases *FGFR2*-IIIb levels while increasing *FGFR2*-IIIc (31). To test for an effect of loss of ESRP1 and ESRP2 on *FGFR2* isoform detection by HCR-RNA-FISH, MCF-7 cells were treated with siRNAs targeting *ESRP1* and *ESRP2* for 72 h, and efficient knock down was confirmed by PCR (Supplementary Figure S9) and HCR-RNA-FISH (Supplementary Figure S10). Single cell data from treated versus untreated cells indicates correlated knock downs of *ESRP1* and *ESRP2* in individual cells (Supplementary Figure S10). While no changes were observed for total *FGFR2* (Figure 5A, D), *FGFR2*-IIIb HCR spot counts were reduced in concomitant *ESRP1* and *ESRP2* knock down cells (Figure 5B, D). No change was observed in the levels of the control housekeeping gene *TBP* (Figure 5C, D). Single cell HCR spot count data for total-*FGFR2* and *FGFR2*-IIIb indicates that while the expression of *FGFR2*-IIIb decreased, the expression pattern of total *FGFR2* remained unchanged between treated and untreated cells (Figure 5E). This observation reinforces the notion that changes in *FGFR2*-IIIb spot count in treated cells are due to changes in *FGFR2* splicing but not to changes in *FGFR2* transcription. In addition, no change was observed between untreated and treated cells for total *FGFR2* and *TBP* spot counts (Figure 5F). These observations demonstrate the ability of HiFENS to accurately detect changes in splicing isoforms in response to experimental perturbations, which are known to lead to changes in AS outcomes for *FGFR2*. This makes the method suitable for targeted mechanistic studies of splicing isoforms.

HCR-RNA-FISH for high throughput screens

A major potential application for isoform-specific HCR-RNA-FISH is in imaging-based functional genomics screens for the discovery of new AS regulators using the detection of endogenous mRNA isoforms as a read-out. To test the suitability of HiFENS for such screens, we used an siRNA library targeting 702 human kinases (Figure 6A). 72 h after siRNA transfection, cells were subjected to HCR-RNA-FISH using probes to detect total *FGFR2* (*FGFR2*-D7-10), *FGFR2*-IIIb and *TBP* in a multiplexed format. Each library gene was targeted by three separate siRNAs which were tested in individual wells. At least 700 cells were imaged per siRNA. *TBP* served as a house-keeping control gene and total *FGFR2* served to distinguish changes in transcription from changes in splicing. As a quality control step, we surveyed spot counts across six imaging plates and spot counts for *FGFR2*-D7-10 (Figure 6B) and *FGFR2*-IIIb (Figure 6C) were found to show very little variation across plates and wells (Figure 6B, C).

We used a median per gene threshold z-score of 1.5 (i.e. at least two out of the three siRNA oligos with a z-score > 1.5 or z-score < 1.5) to identify potential hits (Supplementary Table S2). At this threshold, we found that knockdown of five genes (*COL4A3BP*, *STK36*, *EIF2AK1*, *SMG1* and *SCGB2A1*) significantly reduced *FGFR2*-IIIb levels (Figure 6D, Table 1) as indicated by lower HCR spot count for *FGFR2*-IIIb while the total *FGFR2* HCR spot count was unaffected. siRNA oligos against *SCGB2A1* reduced both *FGFR2*-IIIb and *TBP* levels (Table 1). For 13 knock down target genes, HCR spot count was lower for both *FGFR2*-IIIb and total *FGFR2*, suggesting that the targets are transcriptional repressors of *FGFR2*, rather than changes in regulation of splicing (Figure 6D). Conversely, siRNA oligos against five genes (*CAMK1D*, *MAP2K3*, *MAP3K11*, *VRK1* and *WEE1*) had median z-scores > 1.5 for *FGFR2*-IIIb HCR spot count but not for total *FGFR2*, indicating an increase in the levels of the *FGFR2*-IIIb isoform (Figure 6E, Table 2). Knock down of nine genes had median z-scores >1.5 for both total and *FGFR2*-IIIb, suggesting an activation role for these in the regulation of *FGFR2* transcription (Figure 6E). Taking advantage of the fact that the FGFR proteins are receptor kinases themselves, and that siRNA oligos against their genes were present in the kinome library, we checked the effect of knocking down the expression of *FGFR* family members in the screen. Reassuringly, only *FGFR2* turned out to be a transcriptional hit according to our criteria, since its

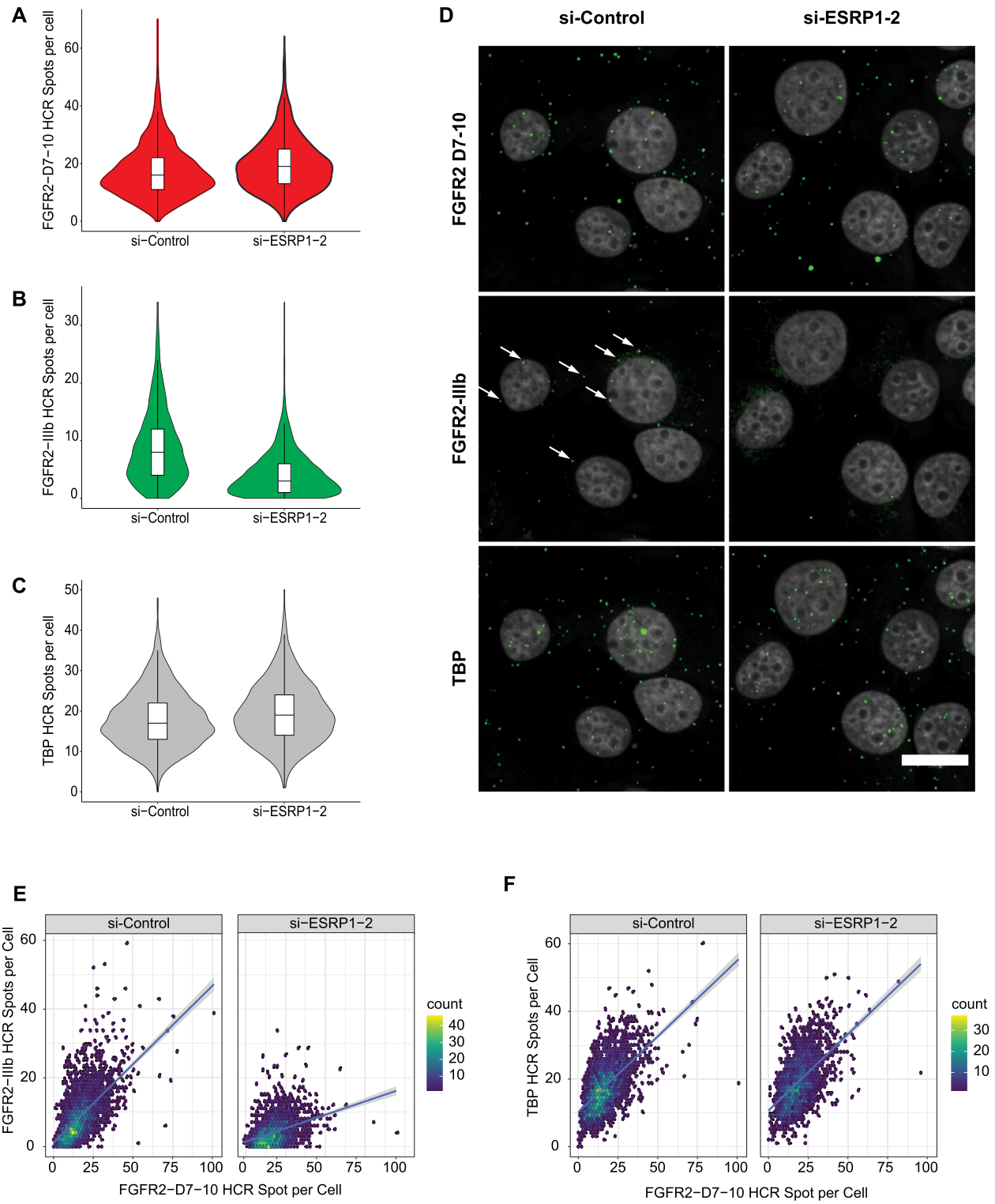

Figure 5. Detection of changes in endogenous *FGFR2* isoforms. (**A–C**) Violin and box plots for RNA-HCR-FISH spot count measurements for multiplexed probes for *FGFR2*-D7-10 (A), *FGFR2*-IIIb (B) and *TBP* (C) in MCF-7 cells. MCF-7 cells were treated with siRNAs against *ESRP1* and *ESRP2* (si-ESRP-1-2) or scrambled siRNA (si-Control). Cells were fixed 72 h post transfection. Boxes show the 25th, 50th (median) and 75th percentile of the distributions and whiskers extend to 1.5X inter-quantile range (IQR). Values are generated from single cell data and are representative of four replicates. At least, 500 cells were analyzed per sample. (**D**) Representative field of view of RNA-HCR-FISH for *FGFR2*-Full, *FGFR2*-IIIb and *TBP* in treated (si-ESRP-1-2) and control (si-Control) MCF-7 cells. White arrows indicate *FGFR2*-IIIb spots. Scale bar: 20 μm. (**E**, **F**) Scatter plots of RNA-HCR-FISH spot count measurements for *FGFR2*-D7-10 (x-axis) and *FGFR2*-IIIb (y-axis) (E) and for *FGFR2*-D7-10 (x-axis) and *TBP* (y-axis) (F) in cells described in (A–C). Number of cells in each plot area is color coded (see legend). Values are generated from single cell data and are representative of four replicates. At least 500 cells were analyzed per sample.

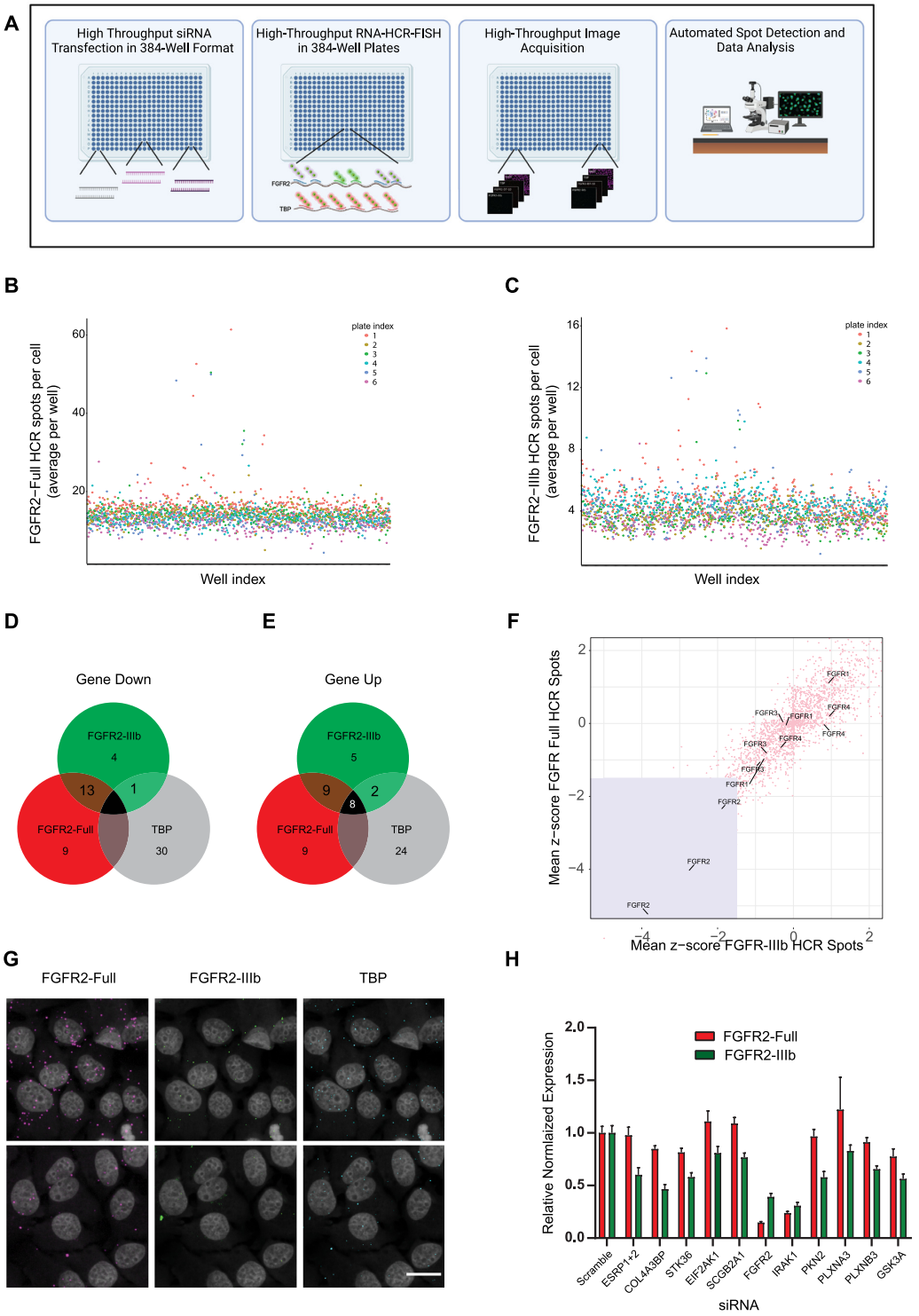

Figure 6. Isoform specific probes for use in high throughput screen. (**A**) Outline of HiFENS pipeline in MCF-7 cells. Reverse siRNA transfection and RNA-HCR-FISH protocols are performed in a 384-well format in a fully automated manner followed by automated image acquisition by high-throughput microscopy. Image analysis is performed using Columbus to identify nuclei, cytoplasm, and spots in each cell (see Materials and Methods for details). (**B**, **C**) Spot count for *FGFR2*-Full (B) and *FGFR2*-IIIb (C) across all six screen plates (plate index) by well position (well index). (**D**, **E**) Venn diagram representation for number of genes that decreased (D) or increased (E) spot counts by 1.5 *z*-score units. (**F**) Scatter plot for mean *z*-scores for FGFRF2-Full (y-axis) and *FGFR2*-IIIb (x-axis). Shaded area highlights plot region in which both *FGFR2*-Full and *FGFR2*-IIIb are lower than 1.5 *z*-score units. Results from all three siRNAs against *FGFR* family members are indicated. (**G**) Representative maximum projection images for *FGFR2*-IIIb in control siRNA well (Si-Control) and siRNA against *FGFR2* (Si-FGFR2). Scale bar: 10 μm. (**H**) Quantitative RT-PCR for *FGFR2*-Full and for the *FGFR2*-IIIb isoform. MCF7 cells were treated with the indicated siRNAs. RNA was harvest ed 72 h post transfection. Expression levels are normalized to expression of *TBP*, and relative to the expression of Scramble siRNA which was arbitrarily set at one. Values represent mean ± SEM of three experiments.

Table 1. Screen Hits for decrease in FGFR2-Full and FGFR2-IIIb levels

	FGFR2-IIIb Screen Hits		FGFR2-Full Screen Hits	
1	**Gene Symbol**	**Median Z-Score**	**Gene Symbol**	**Median Z-Score**
2	CDKL3	-1.7	CDKL3	-1.67
3	COL4A3BP	-1.53	DMPK	-1.77
4	DMPK	-1.56	FGFR2	-4.04
5	EIF2AK1	-1.63	FGGY	-2.04
6	FGFR2	-2.76	GSK3A	-1.74
7	HIPK1	-1.97	HIPK1	-2.4
8	IRAK1	-2.87	IRAK1	-3.18
9	KSR1	-1.75	KSR1	-2.06
10	MAP4K3	-2.15	MAP2K4	-1.62
11	PKN2	-1.75	MAP4K3	-1.83
12	PLK2	-1.74	MPP6	-1.66
13	PLK4	-1.8	PKN2	-2.33
14	PLXNA3	-2.01	PLK2	-1.81
15	PLXNB2	-1.72	PLK4	-1.84
16	SCGB2A1	-1.69	PLXNA3	-1.68
17	SMG1	-1.79	PLXNB2	-2.32
18	STK36	-1.63	RIPK3	-1.56
19	STK38	-1.94	SBK1	-1.97
20			SCYL1	-1.58
21			STK38	-2.11
22			TAF1L	-1.71
23			WNK2	-1.78

Specific Hit
FGFR2-Full + FGFR2-IIIb
FGFR2-IIIb + TBP

knockdown led to a concomitant reduction of HCR spot counts for both *FGFR2*-D7-10 and *FGFR2*-IIIb (Figure 6F, G).

To validate the hits identified in the screen, we tested by qRT-PCR four specific siRNA hits (*COL4A3BP*, *STK36*, *EIF2AK1,* and *SCGB2A1*) which reduced *FGFR2*-IIIb HCR spot counts, along with five siRNA treatments against other genes (*IRAK1*, *PKN2*, *PLXNA3*, *PLXNB3,* and *GSK3A*) which led to reduced total *FGFR2* (Table 2). siRNA oligos against *ESRP1* and *ESRP2* served as positive controls and a scrambled siRNA oligo as the negative control. Knock-down of all four specific hits caused a decrease in *FGFR2*-IIIb levels but not it total *FGFR2* levels, similar to the expression pattern observed in the concomitant knock-down of *ESRP1* and *ESRP2* (Figure 6H). Together, these results are proof-of-principle for the use of HiFENS for the identification of novel AS regulators in unbiased high-throughput screens.

DISCUSSION

Alternative splicing (AS) is regulated at different levels, including cis-regulatory sequence elements and trans-acting splicing factors (42,43). In addition, the activity of splicing factors is regulated by post-translational modifications, in particular phosphorylation (44–46). Changes in splicing factor phosphorylation can influence their localization and binding activity, ultimately affecting splicing outcome (16). Several downstream protein kinase families that use splicing factors as substrates have been characterized and are the targets for therapeutic treatment for different diseases, including cancer (47–49). Yet, the identity and role of upstream kinases and cellular signal transduction pathways in splicing regulation and control of AS are relatively poorly characterized. A major reason for the limited understanding of cellular signaling pathways in AS regulation is the lack of suitable experimental assays to identify relevant signaling components in a systematic fashion, including in unbiased cell-based screens and using endogenous genes as targets. We have developed such a tool in this study.

We have taken advantage of the high sensitivity of HCR to establish an imaging-based pipeline, HiFENS, for quantitative detection of RNA isoforms in a 384-well format using multiplexed HCR probe sets. Our approach is a microscopy-based method that produces single cell data. Importantly, the use of HCR fluorescence signal amplification overcomes the two major limitations of traditional FISH methods for the sensitive detection of endogenous splicing isoforms. First, the use of signal amplification makes it feasible to use lower magnification objectives (such as 40X or 20X), which allow imaging of a large numbers of cells per field of view, an essential condition for high-throughput experiments. Second, while traditional smFISH

Table 2. Screen Hits for increase in FGFR2-Full and FGFR2-IIIb levels

	FGFR2-IIIb Screen Hits		FGFR2-Full Screen Hits	
1	Gene Symbol	Median Z-Score	Gene Symbol	Median Z-Score
2	AK8	1.89	AK8	2.48
3	AURKA	5.97	AURKA	8.63
4	AURKB	6.33	AURKB	6.75
5	BUB1B	26.33	BUB1B	20.32
6	CDC2	13.57	CAMK1D	1.57
7	CDC2L5	1.77	CDC2	11.3
8	CDK11B	4.93	CDC2L5	1.53
9	CSNK1A1	1.9	CDC7	1.87
10	DCLK3	1.58	CDK11B	4.01
11	EPHB1	2.15	CRKRS	2.13
12	GAK	1.86	CSNK1A1	3.76
13	GUK1	1.52	MAP2K3	2.09
14	MPP2	1.68	MAP3K11	1.6
15	NME3	2.16	PACSIN1	1.62
16	PACSIN1	1.63	PASK	3.01
17	PASK	1.99	PHKG2	1.82
18	PDXK	2.23	PLK1	11.64
19	PHKG2	2.24	SCYL3	2.52
20	PLK1	11.06	SPHK2	3
21	PRPS1	1.8	SRPK1	1.82
22	RPS6KB2	1.72	TTK	17.43
23	SCYL3	2.39	UCK2	1.99
24	SPHK2	1.58	VRK1	1.77
25	SRPK1	2.4	WEE1	1.99
26	TTK	22.2		
27				
28	Specific Hit			
29	FGFR2-Full + FGFR2-IIIb			
30	FGFR2-IIIb + TBP			
31	FGFR2-Full + FGFR2-IIIb + TBP			

is limited by the fluorescence signal generated by the number of directly labelled probes that can hybridize to short or rare sequences such as splice junctions or short exons, HCR enables detection of very short target sequences. We demonstrate here that use of HCR provides sensitive and highly specific detection of splicing isoforms in situ (50–53). We used HCR-RNA-FISH to amplify fluorescent signal without sacrificing single molecule resolution. This allows detection of unique sequences for each of the *FGRF2* isoforms. Importantly, the signal obtained from HCR-RNA-FISH depends on the number of probes used. We find that use of as few as 3-4 probe pairs allows accurate quantitative detection of specific *FGFR2* isoforms. The weaker signal of fewer probes is compensated by the reduced background resulting in high signal to noise ratios, especially in the far-red channel. Importantly, HiFENS can be used in a fully automated fashion which is a requirement for high-throughput screens. The routine use of a 384-well plate format enables screening of relatively large libraries. For example, screening of 702 genes as performed in this study could be completed on 6 plates per screening replicate with a total imaging time of ∼30 h.

An important advantage of HiFENS is its ability to detect and probe the behavior of endogenous RNAs rather than artificial reporter genes. The use of endogenous genes as a screening readout eliminates possible artifacts created by reporters and ensures probing of physiological levels of splicing isoforms. We demonstrate the usefulness of hiFENS for discovery of novel splicing regulators in a proof-of-principle screen of an siRNA library of 702 cellular signaling factors. Reassuringly, we find *FGFR2* itself as one of our top hits and PCR validation suggest accu-

rate detection of hits. In addition, we identify and validate several novel potential regulators of *FGFR2* AS, including *STK36*, a ser/thr kinase involved in ciliary and flagellar motility (54) and *SCGB2A1*, a putative marker of chemoresistance in colon cancer (55). Detailed characterization of the identified hits will be the subject of future studies.

HiFENS has limitations. In particular, thedetection of very short or rare RNA sequences remains challenging. In our study, three or four probes were typically sufficient for detection of desired target sequences. While unique sequences of about 200 nt were sufficient for specific detection, isoform probes yielded lower spot count compared to the full-length probes. As a result, our method provides relative, but not absolute, information on isoform levels, and detection of a splicing event involving a cassette exon, which would require detection of a skipped isoform using only one probe spanning the junction of the flanking exons, may therefore be challenging. Consequently, empirical testing for probes combination may be required for each splicing event to get optimal results. Furthermore, while HiFENS is robust, it is anticipated the assay conditions for new targets and cell types may differ considerably requiring in depth assay development and optimization for each target. Finally, while imaging-based approaches are complementary to sequencing based methods to study AS mechanisms, they are limited by the need for a pre-selected RNA target, whereas NGS methods have the potential to discover new RNA transcripts and splice variants. hiFENS does not report on gene activity since spot intensity measurements in the population are too noisy for accurate determination of overall cellular expression levels of the target gene. HCR based approaches also rely on fixed cells and cannot be used for live cell imaging and they can therefore not provide any direct information about expression dynamics, including gene bursting.

Taken together, we report here the development of a novel approach to study AS and to discover novel AS regulators and as such represents a useful tool in understanding the role of AS in physiological and pathological settings.

DATA AVAILABILITY

The R analysis scripts used to generate the plots in the figures are deposited at https://github.com/CBIIT/mistelilab-hifens.

SUPPLEMENTARY DATA

Supplementary Data are available at NAR Online.

FUNDING

Intramural Research Program of the National Institutes of Health (NIH); National Cancer Institute; Center for Cancer Research [1ZIAB010309-23]. Funding for open access charge: National Institutes of Health (NIH); National Cancer Institute; Center for Cancer Research [1ZIAB010309-23].
Conflict of interest statement. None declared.

REFERENCES

1. Bentley,D.L. (2014) Coupling mRNA processing with transcription in time and space. *Nat. Rev. Genet.*, **15**, 163–175.
2. Passmore,L.A. and Coller,J. (2022) Roles of mRNA poly(A) tails in regulation of eukaryotic gene expression. *Nat. Rev. Mol. Cell. Biol.*, **23**, 93–106.
3. Galloway,A. and Cowling,V.H. (2019) mRNA cap regulation in mammalian cell function and fate. *Biochim. Biophys. Acta. Gene. Regul. Mech.*, **1862**, 270–279.
4. Gehring,N.H. and Roignant,J.Y. (2021) Anything but ordinary - emerging Splicing mechanisms in eukaryotic gene regulation. *Trends Genet.*, **37**, 355–372.
5. Ule,J. and Blencowe,B.J. (2019) Alternative splicing regulatory networks: functions, mechanisms, and evolution. *Mol. Cell.*, **76**, 329–345.
6. Kim,E., Goren,A. and Ast,G. (2008) Alternative splicing: current perspectives. *Bioessays.*, **30**, 38–47.
7. Letunic,I., Copley,R.R. and Bork,P. (2002) Common exon duplication in animals and its role in alternative splicing. *Hum. Mol. Genet.*, **11**, 1561–1567.
8. Hatje,K., Rahman,R.U., Vidal,R.O., Simm,D., Hammesfahr,B., Bansal,V., Rajput,A., Mickael,M.E., Sun,T., Bonn,S. *et al.* (2017) The landscape of human mutually exclusive splicing. *Mol. Syst. Biol.*, **13**, 959.
9. Kornblihtt,A.R., Schor,I.E., Allo,M., Dujardin,G., Petrillo,E. and Munoz,M.J. (2013) Alternative splicing: a pivotal step between eukaryotic transcription and translation. *Nat. Rev. Mol. Cell Biol.*, **14**, 153–165.
10. Wilkinson,M.E., Charenton,C. and Nagai,K. (2020) RNA splicing by the spliceosome. *Annu. Rev. Biochem.*, **89**, 359–388.
11. Wan,R.X., Bai,R., Zhan,X.C. and Shi,Y.G. (2020) How is precursor messenger RNA spliced by the spliceosome?*Annu. Rev. Biochem.*, **89**, 333–358.
12. Fu,X.D. and Ares,M. (2014) Context-dependent control of alternative splicing by RNA-binding proteins. *Nat. Rev. Genet.*, **15**, 689–701.
13. Erkelenz,S., Mueller,W.F., Evans,M.S., Busch,A., Schoneweis,K., Hertel,K.J. and Schaal,H. (2013) Position-dependent splicing activation and repression by SR and hnRNP proteins rely on common mechanisms. *RNA*, **19**, 96–102.
14. Prasad,J., Colwill,K., Pawson,T. and Manley,J.L. (1999) The protein kinase clk/sty directly modulates SR protein activity: both hyper- and hypophosphorylation inhibit splicing. *Mol. Cell. Biol.*, **19**, 6991–7000.
15. Naro,C., Bielli,P. and Sette,C. (2021) Oncogenic dysregulation of pre-mRNA processing by protein kinases: challenges and therapeutic opportunities. *FEBS J.*, **288**, 6250–6272.
16. Czubaty,A. and Piekielko-Witkowska,A. (2017) Protein kinases that phosphorylate splicing factors: roles in cancer development, progression and possible therapeutic options. *Int. J. Biochem. Cell. Biol.*, **91**, 102–115.
17. Ruta,V., Pagliarini,V. and Sette,C. (2021) Coordination of RNA processing regulation by signal transduction pathways. *Biomolecules*, **11**, 1475.
18. Orr-Urtreger,A., Bedford,M.T., Burakova,T., Arman,E., Zimmer,Y., Yayon,A., Givol,D. and Lonai,P. (1993) Developmental localization of the splicing alternatives of fibroblast growth factor receptor-2 (FGFR2). *Dev. Biol.*, **158**, 475–486.
19. Holzmann,K., Grunt,T., Heinzle,C., Sampl,S., Steinhoff,H., Reichmann,N., Kleiter,M., Hauck,M. and Marian,B. (2012) Alternative splicing of fibroblast growth factor receptor IgIII loops in cancer. *J. Nucleic Acids*, **2012**, 950508.
20. Goldstrohm,A.C., Greenleaf,A.L. and Garcia-Blanco,M.A. (2001) Co-transcriptional splicing of pre-messenger RNAs: considerations for the mechanism of alternative splicing. *Gene*, **277**, 31–47.
21. Champion-Arnaud,P., Ronsin,C., Gilbert,E., Gesnel,M.C., Houssaint,E. and Breathnach,R. (1991) Multiple mRNAs code for proteins related to the BEK fibroblast growth factor receptor. *Oncogene*, **6**, 979–987.
22. Turner,N. and Grose,R. (2010) Fibroblast growth factor signalling: from development to cancer. *Nat. Rev. Cancer*, **10**, 116–129.
23. Miki,T., Bottaro,D.P., Fleming,T.P., Smith,C.L., Burgess,W.H., Chan,A.M. and Aaronson,S.A. (1992) Determination of ligand-binding specificity by alternative splicing: two distinct growth

factor receptors encoded by a single gene. *Proc. Natl. Acad. Sci. U.S.A.*, **89**, 246–250.
24. Yan,G., Fukabori,Y., McBride,G., Nikolaropolous,S. and McKeehan,W.L. (1993) Exon switching and activation of stromal and embryonic fibroblast growth factor (FGF)-FGF receptor genes in prostate epithelial cells accompany stromal independence and malignancy. *Mol. Cell. Biol.*, **13**, 4513–4522.
25. Matsubara,A., Kan,M., Feng,S.J. and McKeehan,W.L. (1998) Inhibition of growth of malignant rat prostate tumor cells by restoration of fibroblast growth factor receptor 2. *Cancer Res.*, **58**, 1509–1514.
26. Ricol,D., Cappellen,D., El Marjou,A., Gil-Diez-de-Medina,S., Girault,J.M., Yoshida,T., Ferry,G., Tucker,G., Poupon,M.F., Chopin,D. *et al.* (1999) Tumour suppressive properties of fibroblast growth factor receptor 2-IIIb in human bladder cancer. *Oncogene*, **18**, 7234–7243.
27. Luco,R.F., Pan,Q., Tominaga,K., Blencowe,B.J., Pereira-Smith,O.M. and Misteli,T. (2010) Regulation of alternative splicing by histone modifications. *Science*, **327**, 996–1000.
28. Shapiro,I.M., Cheng,A.W., Flytzanis,N.C., Balsamo,M., Condeelis,J.S., Oktay,M.H., Burge,C.B. and Gertler,F.B. (2011) An EMT-driven alternative splicing program occurs in human breast cancer and modulates cellular phenotype. *PLoS Genet.*, **7**, e1002218.
29. Mauger,D.M., Lin,C. and Garcia-Blanco,M.A. (2008) hnRNP H and hnRNP F complex with fox2 to silence fibroblast growth factor receptor 2 exon IIIc. *Mol. Cell. Biol.*, **28**, 5403–5419.
30. Gesnel,M.C., Del Gatto-Konczak,F. and Breathnach,R. (2009) Combined use of MS2 and PP7 coat fusions shows that TIA-1 dominates hnRNP A1 for K-SAM exon splicing control. *J. Biomed. Biotechnol.*, **2009**, 104853.
31. Warzecha,C.C., Sato,T.K., Nabet,B., Hogenesch,J.B. and Carstens,R.P. (2009) ESRP1 and ESRP2 are epithelial cell-type-specific regulators of FGFR2 splicing. *Mol. Cell.*, **33**, 591–601.
32. Topp,J.D., Jackson,J., Melton,A.A. and Lynch,K.W. (2008) A cell-based screen for splicing regulators identifies hnRNP LL as a distinct signal-induced repressor of CD45 variable exon 4. *RNA*, **14**, 2038–2049.
33. Stoilov,P., Lin,C.H., Damoiseaux,R., Nikolic,J. and Black,D.L. (2008) A high-throughout screening strategy identifies cardiotonic steroids as alternative splicing modulators. *Proc. Natl. Acad. Sci. U.S.A.*, **105**, 11218–11223.
34. Lin,J.H., Wu,H., Zou,W.B., Masson,E., Fichou,Y., Le Gac,G., Cooper,D.N., Ferec,C., Liao,Z.A. and Chen,J.M. (2021) Splicing outcomes of 5 ' splice site GT >GC variants that generate wild-type transcripts differ significantly between full-length and minigene splicing assays. *Front. Genet.*, **12**, 701652.
35. Pegoraro,G. and Misteli,T. (2017) High-throughput imaging for the discovery of cellular mechanisms of disease. *Trends Genet.*, **33**, 604–615.
36. Waks,Z., Klein,A.M. and Silver,P.A. (2011) Cell-to-cell variability of alternative RNA splicing. *Mol. Systems Biol.*, **7**, 506.
37. Chen,K.H., Boettiger,A.N., Moffitt,J.R., Wang,S.Y. and Zhuang,X.W. (2015) RNA imaging.Spatially resolved, highly multiplexed RNA profiling in single cells. *Science*, **348**, aaa6090.
38. Erben,L., He,M.X., Laeremans,A., Park,E. and Buonanno,A. (2018) A novel ultrasensitive in situ hybridization approach to detect short sequences and splice variants with cellular resolution. *Mol. Neurobiol.*, **55**, 6169–6181.
39. Choi,H.M.T., Schwarzkopf,M., Fornace,M.E., Acharya,A., Artavanis,G., Stegmaier,J., Cunha,A. and Pierce,N.A. (2018) Third-generation in situ hybridization chain reaction: multiplexed, quantitative, sensitive, versatile, robust. *Development*, **145**, dev165753.
40. Dirks,R.M. and Pierce,N.A. (2004) Triggered amplification by hybridization chain reaction. *Proc. Natl. Acad. Sci. U.S.A.*, **101**, 15275–15278.
41. Schwarzkopf,M., Choi,H.M.T. and Pierce,N.A. (2020) Multiplexed quantitative in situ hybridization for mammalian cells on a slide: qHCR and dHCR imaging (v3.0). *In Situ Hybridization Protocols, 5 Edition*, **2148**, 143–156.
42. Barash,Y. and Vaquero-Garcia,J. (2014) Splicing code modeling. *Syst. Biol. RNA Binding Proteins*, **825**, 451–466.
43. Yeo,G.W. (2014) Systems biology of RNA binding proteins preface. *Syst. Biol. RNA Binding Proteins*, **825**, V–VII.
44. Naro,C. and Sette,C. (2013) Phosphorylation-mediated regulation of alternative splicing in cancer. *Int. J. Cell. Biol.*, **2013**, 151839.
45. Zhou,Z. and Fu,X.D. (2013) Regulation of splicing by SR proteins and SR protein-specific kinases. *Chromosoma*, **122**, 191–207.
46. Blaustein,M., Pelisch,F., Tanos,T., Munoz,M.J., Wengier,D., Quadrana,L., Sanford,J.R., Muschietti,J.P., Kornblihtt,A.R., Caceres,J.F. *et al.* (2005) Concerted regulation of nuclear and cytoplasmic activities of SR proteins by AKT. *Nat. Struct. Mol. Biol.*, **12**, 1037–1044.
47. Corkery,D.P., Holly,A.C., Lahsaee,S. and Dellaire,G. (2015) Connecting the speckles: splicing kinases and their role in tumorigenesis and treatment response. *Nucleus*, **6**, 279–288.
48. Moyano,P.M., Nemec,V. and Paruch,K. (2020) Cdc-Like kinases (CLKs): biology, chemical probes, and therapeutic potential. *Int. J. Mol. Sci.*, **21**, 7549.
49. Czubaty,A. and Piekielko-Witkowska,A. (2017) Protein kinases that phosphorylate splicing factors: roles in cancer development, progression and possible therapeutic options. *Int. J. Biochem. Cell. B.*, **91**, 102–115.
50. Wang,Y.S. and Guo,J. (2021) Multiplexed single-cell in situ RNA profiling. *Front. Mol. Biosci.*, **8**, 775410.
51. Rouhanifard,S.H., Mellis,I.A., Dunagin,M., Bayatpour,S., Jiang,C.N.L., Dardani,I., Symmons,O., Emert,B., Torre,E., Cote,A. *et al.* (2019) ClampFISH detects individual nucleic acid molecules using click chemistry-based amplification (vol 37, pg 84, 2018). *Nat. Biotechnol.*, **37**, 102–102.
52. Kishi,J.Y., Lapan,S.W., Beliveau,B.J., West,E.R., Zhu,A., Sasaki,H.M., Saka,S.K., Wang,Y., Cepko,C.L. and Yin,P. (2019) SABER amplifies FISH: enhanced multiplexed imaging of RNA and DNA in cells and tissues. *Nat. Methods*, **16**, 533–544.
53. Beliveau,B.J., Boettiger,A.N., Avendano,M.S., Jungmann,R., McCole,R.B., Joyce,E.F., Kim-Kiselak,C., Bantignies,F., Fonseka,C.Y., Erceg,J. *et al.* (2015) Single-molecule super-resolution imaging of chromosomes and in situ haplotype visualization using oligopaint FISH probes. *Nat. Commun.*, **6**, 7147.
54. Edelbusch,C., Cindric,S., Dougherty,G.W., Loges,N.T., Olbrich,H., Rivlin,J., Wallmeier,J., Pennekamp,P., Amirav,I. and Omran,H. (2017) Mutation of serine/threonine protein kinase 36 (STK36) causes primary ciliary dyskinesia with a central pair defect. *Hum. Mutat.*, **38**, 964–969.
55. Munakata,K., Uemura,M., Takemasa,I., Ozaki,M., Konno,M., Nishimura,J., Hata,T., Mizushima,T., Haraguchi,N., Noura,S. *et al.* (2014) SCGB2A1 is a novel prognostic marker for colorectal cancer associated with chemoresistance and radioresistance. *Int. J. Oncol.*, **44**, 1521–1528.